Journal of Hydroscience and Hydraulic Engineering
Vol. 24, No. 2 November, 2006, 41-51

Surface oscillations in flow past a side cavity using stereoscopic measurement and POD

By

R. Tsubaki

COE program researcher, Graduate School of Science and Technology,
Kobe University, Rokkodai, Nada, Kobe, Hyogo, Japan

and

I. Fujita

Professor, Department of Architecture and Civil Engineering,
Kobe University, Rokkodai, Nada, Kobe, Hyogo, Japan

SYNOPSIS

When a relatively large side cavity is created in an open channel, the influence of vortices in the shear layer and circulatory flow is exerted on the main flow, causing surface oscillations and increased water levels. The mechanism of the oscillation is still not clearly understood because of the complexity of the phenomena. In this research, by using a stereoscopic surface measurement system developed by the authors, time-dependent water surface configurations are successfully measured at a sampling rate of 12 Hz, from which general features of the surface oscillation are made clear for a wide range of Froude numbers. Then, we applied the proper orthogonal decomposition (POD) method to measure results. We found that the surface oscillation can be clearly decomposed into a seiche-like major mode and sub-modes with smaller wavelengths.

INTRODUCTION

To maintain public accessibility to waters, side cavities and stairs are created in several rivers in urbanized areas in Japan (Fig. 1). These structures could be at risk due to the rise of water-level during floods; thus, the prediction of flow around this shape is an important matter to be considered. Both experimental evaluation and estimation by computational fluid dynamics (CFD) play prominent roles in prediction of flows and in the design process for river planning. In short, to estimate the flow past a side cavity, the feedback loop involving disturbance between the inner flow and the free surface must be clearly understood.

The free-surface oscillations in the flow past a cavity have some analogy to that of compressible flow. Rockwell and Naudascher (8, 9) reviewed self-sustained oscillations of free shear layers in compressible flow. Rossiter (10) and Rowley *et al.* (11) pointed out that the cavity oscillation arises from such a feedback loop. The feedback loop consists of (A) the growth of instabilities (vortices) in the shear layer, (B) the conversion of vortical disturbances into acoustic waves at the trailing edge, (C) the upward propagation of waves and (D) re-conversion to vortical disturbances at the leading edge. From the above observation, it appears that the velocity field and wave propagation should interact with each other. However, the interactions of the flow field with acoustic pressure variations and surface waves are not identical, especially if the flow has a strong three-dimensionality. The existence of the wall across the cavity in the open channel flow is another important difference. In the study on compressible flow, the opposite side off the cavity is open.

In this research, we measured time-dependent water surface configurations to investigate the mechanisms of oscillation for the purpose of (i) evaluating CFD models regarding the interaction among the geometrical structure, the flow and the water surface oscillation and (ii) the safe and appropriate design of river structures. The surface profiles were measured by using a stereo-scopic surface measurement system developed by the authors. We then applied the proper orthogonal decomposition (POD) method to the measured data.

Fig. 1: River flow past a side cavity during the low-water period

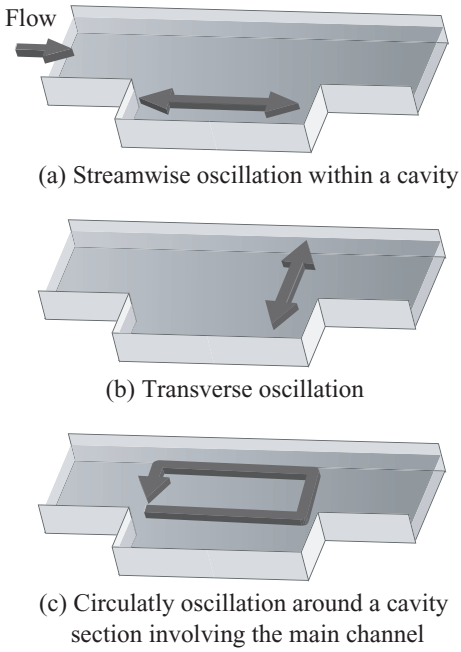

(a) Streamwise oscillation within a cavity

(b) Transverse oscillation

(c) Circulatly oscillation around a cavity section involving the main channel

Fig. 2: Three feedback loops

This paper is organized as follows: Following section presents a brief introduction to the surface fluctuation of a flow through a side cavity. Third section describes the experimental setup and flow conditions that were used in this study. Fourth section presents a brief introduction to POD, in particular, how to observe the propagation of a wave profile by POD. Sixth section describes the results of POD application to the measured value. Then, we draw conclusions in the last section.

SURFACE FLUCTUATION IN A FLOW PAST A SIDE CAVITY

In a flow through a straight channel with a side cavity, the feedback loop may contain not only vortices and waves but also wave reflection off the wall across the cavity. We assume three feedback loops as shown in Fig. 2. The stream-wise oscillation (Fig. 2a) has a feedback loop within the shear layer region (8). This oscillation is subject to intense pressure fluctuations in aeronautics. Kimura and Hosoda (6) reported that this kind of oscillation (Fig. 2a) arises in the hydraulic fields. They carried out experiments using a straight channel with a side cavity and measured oscillation around a side cavity. In Addition, by using numerical results which are validated by the experimental one, they investigated the relation between the Froude number and a surface fluctuation intensity, and found that in the case of specific Froude number such as $Fr = 1, 1/3, 1/5, ..$, a large surface fluctuation comes up. They pointed out that such large fluctuation arises in specific arrangement of large-scale vortices because such arrangement of vortices enhance mass exchange along the interface between the cavity and the main channel.

The transverse oscillation(Fig. 2b) arises in the following loop: (i) vortices approach the downstream edge of a cavity and generate surface waves, (ii) the waves propagate toward the opposite side which are reflected back by the wall of channel. Lastly, (iii) the generated wave affects the approach of a subsequent vortex to the downstream edge.

The circulatory oscillation around a cavity(Fig. 2c) is similar to that of the stream-wise oscillation, but the influence of the wave propagation does not extend within the cavity but through the main channel. In this case, the feedback loop is formed by (i) the development of vortices in the shear layer, (ii) vortices hitting to the edge of the forward facing step followed by disturbance of the surface, (iii) the transmission and reflection of the wave in the upstream direction and (iv) the effect of the vortices at the leading edge of the cavity.

Either way, wave propagation plays a prominent role in feedback loops. Furthermore, these three oscillations may appear either together or individually depending on the hydraulic conditions. We investigate the spatio-temporal deformation of the water surface by means of POD to identify the relationship between the surface fluctuation pattern and the flow parameters (the Froude number and the water depth).

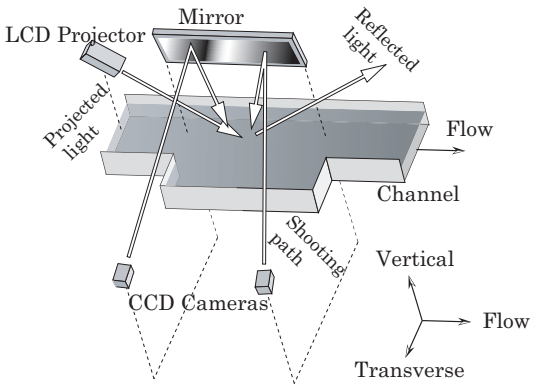

Fig. 3: Experimental setup

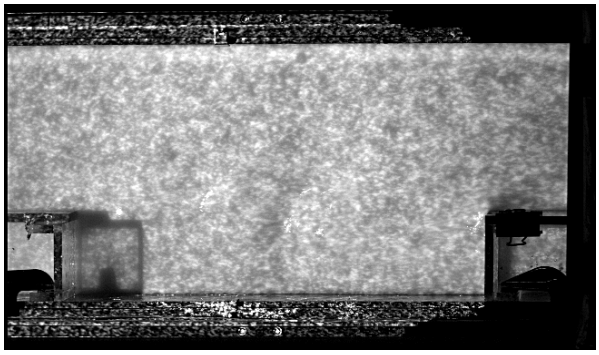

Fig. 4: Captured image. Irregular pattern is projected onto water surface, which is colored white.

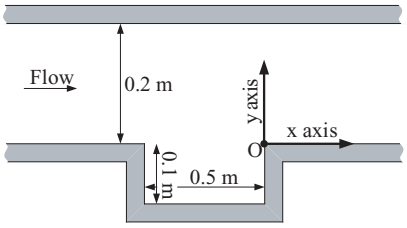

Fig. 5: Plan view of the flume with a cavity

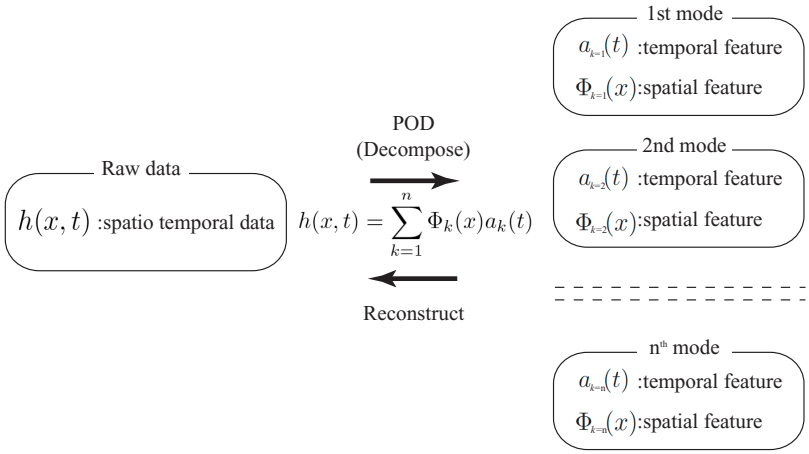

Fig. 6: Schema of proper orthogonal decomposition(POD)

EXPERIMENTAL SETUP

We developed a method for measuring time-varying behavior of the water surface profile (see Tsubaki and Fujita (12, 13)). This method uses a pair of sequential images captured by two high-resolution CCD cameras arranged in a stereo position. The purpose of the method is to make the water color white so that the instantaneous water surface appears like a solid surface with a clear pattern when an irregular pattern of light is projected onto it. It should be noted that this method is suitable for measuring small waves accurately and at the same time discontinuous surfaces robustly. Fig. 3 shows the experimental setup. We used two CCD cameras (KP-F100s, Hitachi Denshi co.), each with a spatial resolution of 1304 by 1024 pixels and a temporal resolution of 12 frames per second. Each pixel of the CCD camera has 8 bit gray scale information. One hundred and fifty images can be captured consecutively with this system. To illuminate the water surface, we used a LCD projector (VPL-CS4, SONY). The resolution of this projector is 800 by 600 pixels; the brightness is 1000 ANSI (Lumen). The projected pattern is shown in Fig. 4. This irregular pattern is designed to maximize the accuracy of a pattern matching process based on the cross-correlation technique within whole measuring area (see e.g. Raffel *et al.* (7)).

Experiments were conducted using a 7.5 m length open-channel flume with a main channel width of 0.2 m. The side-cavity was set up in the middle of the inclined flume. The typical water depth was set to 0.04, 0.06, 0.08 and 0.10m to investigate dependency of 3-Dimensional effect and Reynolds number for surface oscillation. The Froude number was also changed in the range between 0.15 and 1.05. The bottom slope and the flow rate were determined to simulate the intended water depth and Froude number. Fig. 5 shows the coordinate system and configuration of the cavity.

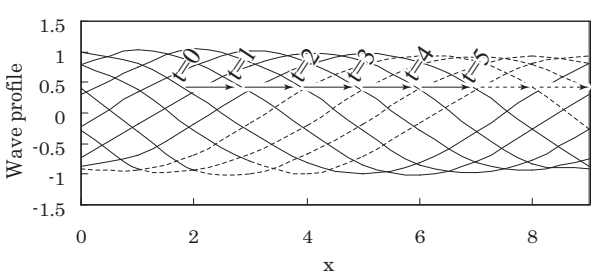

Fig. 7: Wave propagation in one-dimensional space

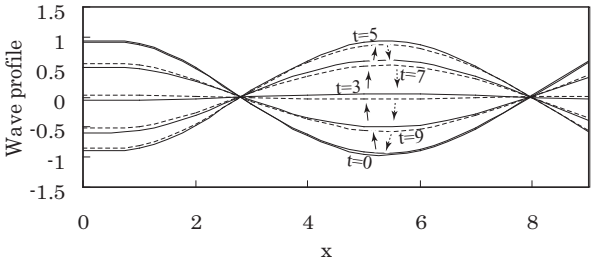

Fig. 8: Time series of re-constructed wave profile of a POD mode

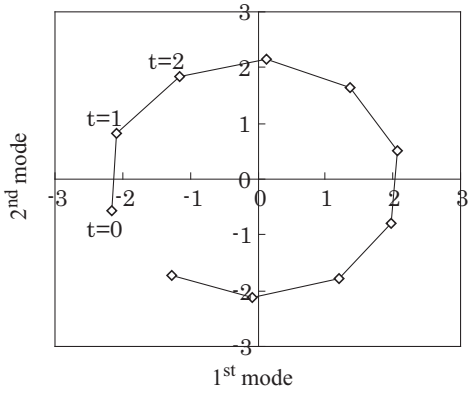

Fig. 9: Phase space projections of temporal amplitude coefficients $a_k(t)$

PROPER ORTHOGONAL DECOMPOSITION

We use the POD method to extract dominant spatial features directly from the measured data. POD is a powerful and well-known technique of making data analysis whose purpose is to obtain low-dimensional approximate descriptions of complex processes(11, 3, 2, 4). Here, we consider a data set of water depth $h(x,t)$ as a function of space x and time t. POD determines the functions $\Phi_k(x)$ and $a_k(t)$ that have the smallest error in the following equation up to the first n^{th} functions(modes),

$$h(x,t) = \sum_{k=1}^{n} \Phi_k(x) a_k(t) + error \tag{1}$$

The functions Φ_k are computed by solving the Fredholm integral equation

$$\int K(x,y)\Phi(y)dy = \lambda\Phi(x) \tag{2}$$

where the kernel $K(x,y) = E(h(x,t)h(y,t))$, which is also the averaged autocorrelation function $K(x,y) = R(x,y)$. In practice, the data is discretized in both space and time. In this case, the integral in Eq. 2 reduces to a standard eigenvalue problem. Here, Φ_k are spatial coefficients called POD modes (eigenfunctions) and the temporal coefficients, $a_k(t)$, are calculated by projecting the data set onto each of the eigenfunctions

$$a_k(t) = (h(x,t), \Phi_k(x)) \tag{3}$$

The eigenvalue λ in Eq. 2 is also called POD energy. The POD mode having the largest λ is called the first mode, and the mode with the second largest λ is called the second mode, and so on.

POD is based on linear combinations of basis functions. POD cannot distinguish between a featureless cloud of points on some plane and a circle on the same plane(3). While the rotary motion obviously has a one-dimensional description, POD might conclude that this motion has two dominant modes. The propagation of a wave is also separated and described by at least two POD modes as discussed in the following section:

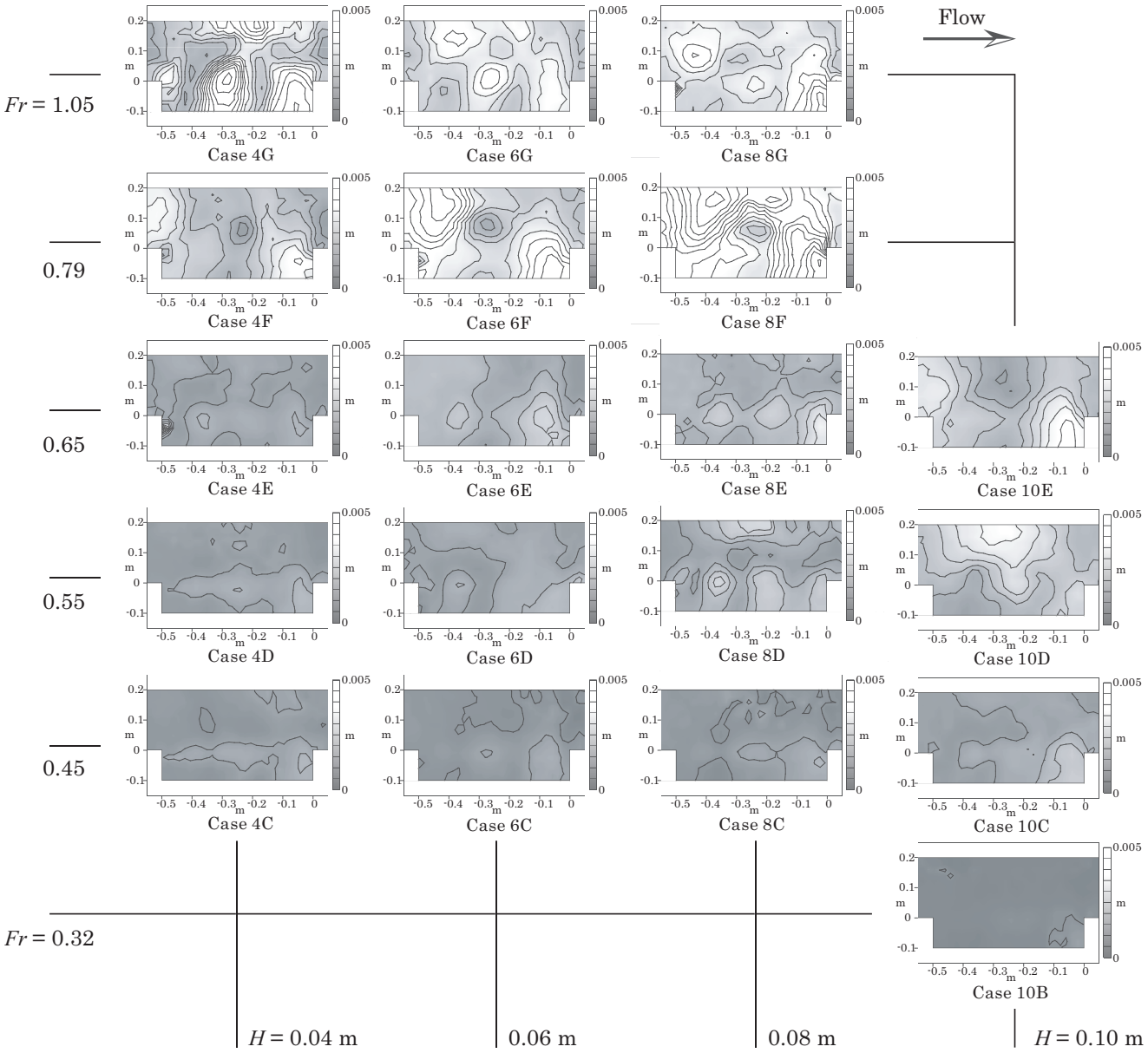

Fig. 10: Intensity of free-surface fluctuation. The Froude number decreases from top to bottom, and the water depth increases from left to right

POD for wave propagation in one-dimensional space

To verify characteristics of POD analysis, wave propagation in one-dimensional space is analyzed by means of POD. The wave has an amplitude of two, a wavelength of ten and a phase speed of one as follows;

$$y = \cos(\frac{x-t}{5}\pi) \tag{4}$$

The time-series of wave profiles are shown in Fig. 7. POD separates this wave into two modes. Each mode has the same POD energy. The reconstructed time dependent profiles of one of the modes is depicted in Fig. 8, the profiles of the other have a quarter wavelength phase shift in space and a $\pi/2$ phase shift in time. The original wave profile consists of the composite wave of both modes. Fig. 9 shows the phase projections of the two temporal amplitude coefficients ($a_k(t)$ in Eq. 1). The phases of each mode are shifted by $\pi/2$, thus a circular pattern is generated in this plot.

Therefore, since the propagation of a wave is divided into two (or more) modes, the phase correlation between all modes must be examined, and the modes that are related must be combined to reconstruct the actual behavior of the waves.

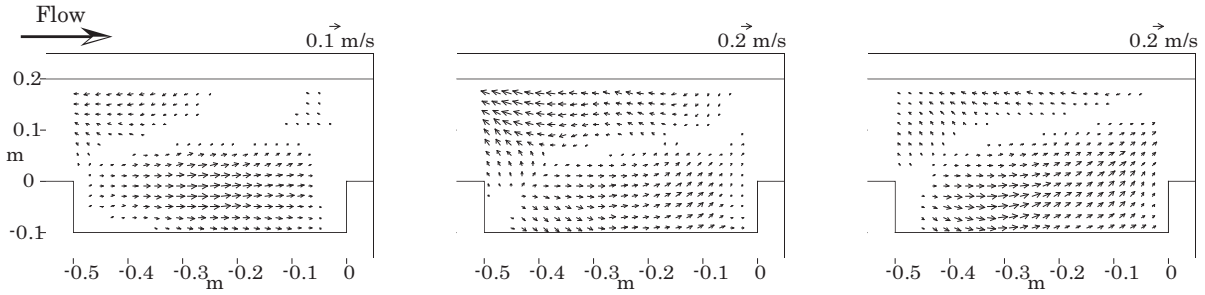

(a) Case 8C (b) Case 8F (c) Case 8G

Fig. 11: Propagation of surface pattern

RESULTS AND DISCUSSIONS

Experiments were performed in the water channel described in second section. First, we discuss profiles of intensity of the surface fluctuation and then we identify the structure of fluctuations (feedback loops) through POD analysis.

Intensity of surface fluctuation

Fig. 10 shows profiles of intensity of the surface fluctuation. The result can be categorized into three types by the Froude number. For the cases where the Froude number is smaller than 0.6, the profiles have some local maxima in the fluctuating region between the leading edge and the downstream edge of the cavity (see e.g. cases 4D and 8D). In this area, vortices develop and travel in a downstream direction, and the water surface sinks at the center of each of the vortices. Furthermore, the seiche-like waves within the cavity resonate with the vortices so that an array of the local maxima appears in the shear layer in this case.

For the cases of $0.6 < Fr < 0.8$, both the downstream area within the cavity and the main channel around the upstream edge of the cavity are oscillating intensively (see e.g. Case 6F and 8F).

Finally, in cases where the Froude number larger than 0.8, several local maxima appear in the shear layer region (see e.g. Case 4G and 8G). The waves can scarcely propagate upward because of the high Froude number and, thus, the circulatory feedback loop can barely be formed. Therefore, seiche-like oscillations arise predominantly in these cases.

Propagation of surface pattern

To identify and visualize the structure of the surface oscillation, propagation velocity of surface pattern is calculated in the following manner. To measure velocity distribution of the flow, visualization technique is widely used. Optical flow method (1, 5) is one of the most important technologies in the motion measurement using the visualization technique. In this method, the distribution of luminance is assumed to convect along with local velocity, then the local velocity is calculated by solving the advection equation for spatial and temporal luminance distributions. Thus, we assume that surface profiles are convected along with local propagation velocity which maintains its pattern within a short period of time, and local propagation velocity is calculated by sequential surface profiles. Spatial distribution of the surface profile is gridded into 0.02 m spacing to calculate the spatial gradient term of the advection equation, and one hundred and fifty frames with 12 FPS (frame per second) interval is used to calculate temporal gradient term.

Fig. 11 shows propagation of surface pattern for Case 8C, 8F and 8G. In Case 8C (Fig. 11a), the downstream velocity is shown in the shear layer region between the main channel and a cavity. In Case 8F (Fig. 11b), the surface profile shifts downstream within the cavity as same as in Case 8C, and going upstream on the other side of the cavity (main channel). Consequently, the circulatory type feedback loop (Fig. 2a) is formed in this case clearly. Finally, in Case 8G (Fig. 11c), a downstream shift around shear layer region becomes strong but a upstream convection is weaken compared than Case 8F. The weakening of the upstream convection in the main channel is caused by high Froude number of the flow, and this weakening has an impact on not only the local flow but also feedback loop of the fluctuation. Thus, downward and upward propagations are both essential to forming a feed back loop, so that the weakening of the upward propagation weakens the feed-back loop itself.

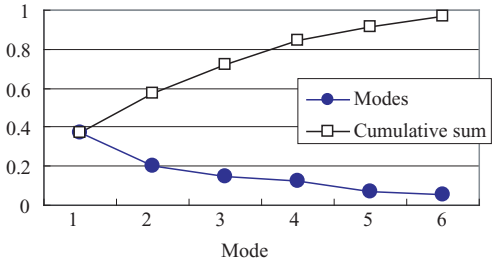

Fig. 12: POD energy spectrum of Case 8C

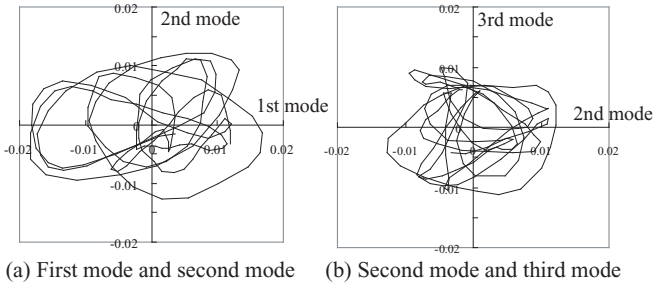

(a) First mode and second mode (b) Second mode and third mode

Fig. 13: Phase space projections of Case 8C

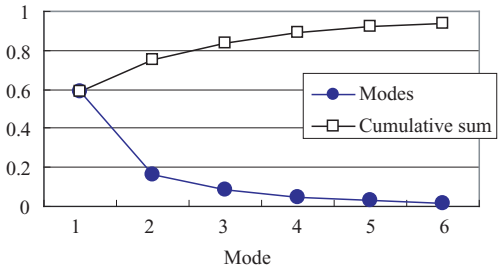

Fig. 14: POD energy spectrum of Case 8F

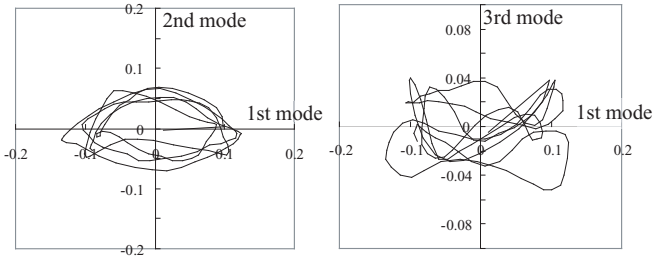

(a) First mode and second mode (b) First mode and third mode

Fig. 15: Phase space projections of Case 8F

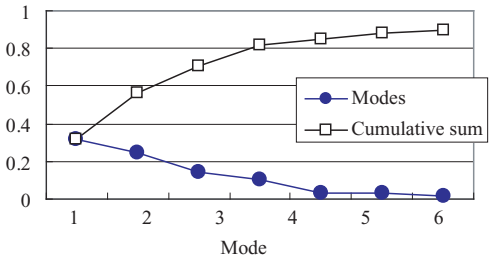

Fig. 16: POD energy spectrum of Case 8G

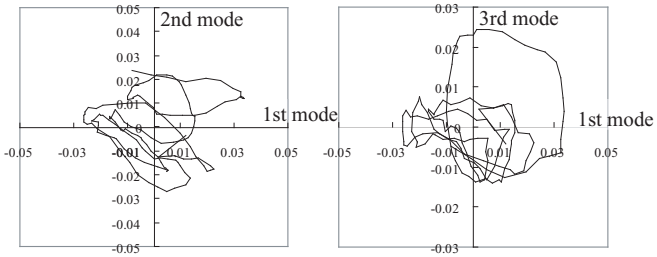

(a) First mode and second mode (b) First mode and third mode

Fig. 17: Phase space projections of Case 8G

POD analysis

To identify each type of spatio-temporal behavior, the POD is applied to the above-mentioned three types of oscillations, and their results are examined in the following sections:

Case 8C: $Fr < 0.6$

The POD energy spectrum of the sampled variables is shown in Fig. 12. This spectrum shows that about 40 % of the POD energy is captured by the first mode and more than 90 % is captured by the first five modes. This suggests that the temporal dynamics of the fluctuation is comparatively simple in the same way as the low dimensionality of the gas pressure in compressible flows compared to that of the velocity components described by Rowley *et al* (11). The phase projections of two amplitude coefficients are demonstrated in Fig. 13 and they reveal the correspondence of the 1st mode with the 2nd mode, 2nd mode with 3rd mode and 3rd mode with 5th mode(omitted in the figure).

The wave propagation reconstructed by the 1st and 2nd modes reveals a circulatory oscillation structure. The sum of the POD energy of the 1st and the 2nd mode contains 60 % of the total energy, indicating that the circulatory oscillation is the key oscillation in this case.

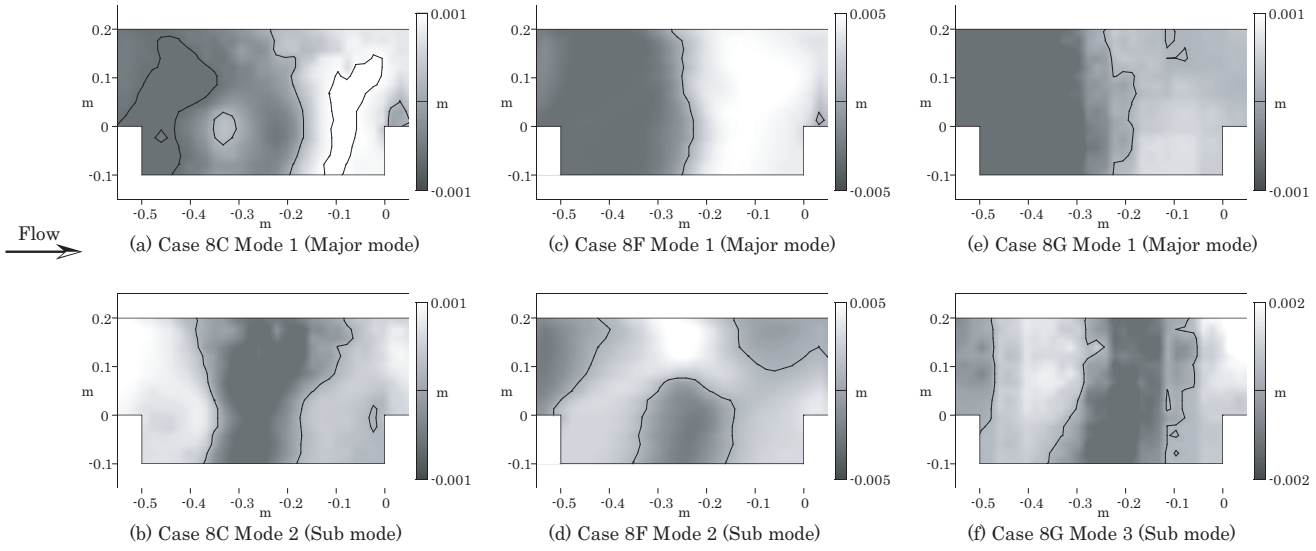

Fig. 18: Major (1st) mode and sub (harmonized to 1st) mode

Case 8F: $0.6 < Fr < 0.8$

The ratio of energy for each POD mode is shown in Fig. 14. The first mode captures more than 60 % of the total POD energy. The first mode has a free surface profile that oscillates from high to low about an axis of symmetry in the center of the cavity (x = -0.25 m). Therefore, the first mode causes intense oscillation both in the downstream area within the cavity and in the upstream area of the main channel as shown in Cases 4F, 6F and 8F of Fig. 10.

Fig. 15 shows the phase space projections, indicating a close correspondence between the 1st and the 2nd modes. The combination of the 1st and the 2nd modes shows a circulatory fluctuation in the time-series of the surface profiles.

Case 8G: $0.8 < Fr$

The POD energy spectrum in this case is shown in Fig. 16. The increment of cumulative POD energy is the slowest among the three cases. The phase space projections (as shown in Fig. 17) also suggest low coherence among modes. An especially weak relation was observed between the 1st and the 3rd modes.

Major mode and sub mode

The three types of oscillation are individually discussed above. In this section, we investigate the relativity between the major (1st mode) and the sub mode which is corresponded with the major mode. Fig. 18 shows the major and sub modes of the three cases. It is apparent that the major modes can describe the spatial features well by representing the seiche-like global oscillation in the stream-wise direction around a side-cavity. As for the features of the sub mode, the wave length becomes approximately two thirds of the length of the side-cavity (0.5m), which is smaller than that of the major mode. The combination of the main mode and the sub mode describes the propagation of the waves. Hence, the seiche-like oscillation is a basic feature of the fluctuation of a flow through a side cavity. This wave is basically a stationary vibration. Furthermore, the sub mode combined with the major mode represents propagation of the waves.

Several local minima and maxima are found in the shear layer region in the case of low Froude number flow (Fig. 18a, b). These show depression of the surface caused by vortices.

In Case 8F (Fig. 18c, d), a checker board pattern appears in a profile of the sub mode. This structure has two nodes along the cavity and one node across the channel. In this case, the major mode contains 60 % of the total energy, which is relatively large compared to the other cases. In addition, the medium Froude number cases show strong oscillation in the upper and lower areas of the side cavity (see Fig. 10). Therefore, the seiche-like oscillation dominates the surface fluctuation (moreover fluctuation of the flow) in the case where the Froude

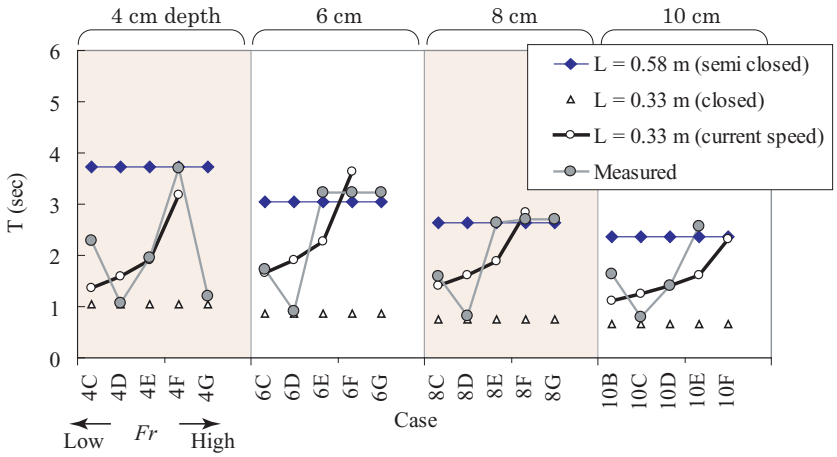

Fig. 19: Wave lengths and periods

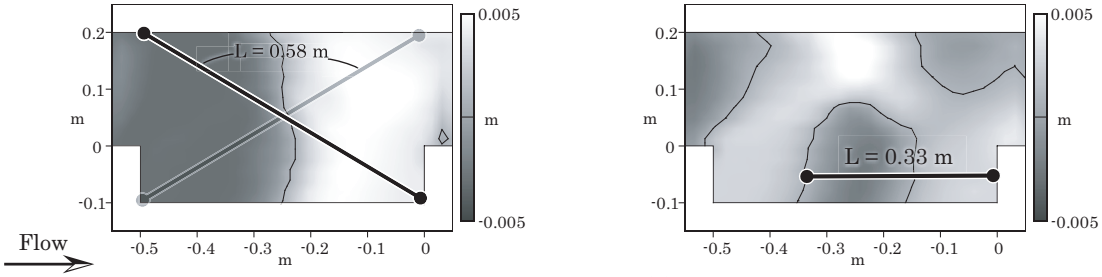

(a) Wave length of seiche in semi enclosed area (Case 8F Mode 1).

(b) Wave length of seiche in enclosed area (Case 8F Mode 2).

Fig. 20: Wave lengths

number is in the range of 0.6 to 0.7 in our experiments.

Frequency and wave length

In addition to the spatial features of the surface oscillation discussed previously, an examination of the oscillation mode frequency and wave length is made in the following section, especially with respect to Froude number. Fig. 19 is a schematic diagram showing the relationship between measured and estimated dominant periods. The measured period T indicates the peak frequency of the temporal coefficient $a_k(t)$ of the major mode. It can be seen that the change of the measured period with respect to the Froude number shows a similar pattern irrespective of water depth, which means 3-Dimensional flow structure and the Reynolds number have little influence on surface oscillation.

Three theoretical periods are also shown in Fig. 19. Wave lengths used in such theoretical periods are determined by using spatial pattern of the major and sub modes extracted by POD analysis as shown in Fig. 20. The first period is generated by the seiche in the semi closed basin and can be calculated by using the following equation:

$$T = \frac{4L}{(2n-1)\sqrt{gh}} \tag{5}$$

where T = period; L = wave length; n = oscillation mode; and g = acceleration due to gravity. The second period corresponds to the seiche interval within a closed area(corresponding to the feedback loop shown in Fig. 2 (a)) and can be expressed as follows:

$$T = \frac{2L}{n\sqrt{gh}} \tag{6}$$

The third period is that of the seiche taking the flow velocity into account (representing the feedback loop shown in Fig. 2 (c)), which is obtained by following equation:

$$T = \frac{L}{n(\sqrt{gh} + v)} + \frac{L}{n(\sqrt{gh} - v)} \tag{7}$$

where v = current velocity in the main channel.

The measured values coincide well with the theoretical values. The periods of the seiche in the semi closed area (Eq. 5) with L = 0.58 m show good agreement with the measured values (in the medium and high Froude number cases at each water depth). Periods calculated by Eq. 7 also show close agreement with measured values within the range of Froude numbers.

Meanwhile. Kimura and Hosoda (6) suggested that surface oscillation is enhanced in the case of oscillation period is resonate with the seiche in the closed area, which period can be expressed by Eq. 6 with wave length is cavity open length which corresponds L = 0.5 0m with our set up. However, the period of such seiche in the closed area with L = 0.50 m is shorter than that of L = 0.33 m and these periods disagree on measured periods of major mode for any case (see Fig. 19. There are no values which are lower than L = 0.33 m in closed seiche). Furthermore, in the case with intense fluctuation ($0.6 < Fr < 0.8$, Case *F), measured periods are considerably larger than that of predicted value by Eq. 6 with L = 0.50 m, so that such intense fluctuation observed in our experiment is not accounted for by Kimura and Hosoda's method in termes of fluctuation periods.

Therefore, surface oscillation in the low Froude number cases may be mainly dominated by the feedback loop due to the stream-wise oscillation within a cavity. However, in the medium Froude number cases, the period of oscillation becomes longer than that of the low Froude number cases, and can be predicted by the equation of the seiche within a semi closed area. Also, the seiche considering the main flow velocity resonates with the semi closed oscillation and consequently intense surface fluctuations occur.

Transverse phase reversal is not seen in Fig. 18 and transverse velocity is not clearly seen in Fig. 11 so that transverse oscillation (Fig. 2 (b)) does not play important role in our case.

CONCLUSION

We measured the surface fluctuation in a flow through a straight open-channel with a side cavity by using a sophisticated stereoscopic image analysis. Instantaneous surface profiles were consecutively obtained by this method, and then decomposed into several modes by means of POD analysis. The distributions of the intensity of surface fluctuations are categorized into three patterns by the Froude number of the flow. The continuous motion of the surface profiles was investigated and waves propagating downstream within the shear layer region were found in low and high Froude number cases. These waves are associated with traveling vortices in the shear layer. From the results of POD analysis, the surface oscillation can be decomposed into a seiche-like major mode and a sub-mode with a smaller wavelength. In the medium Froude number cases, intense fluctuation can be accounted for by the resonance of two modes of seiche with different wave lengths.

Further research is necessary for the development of a simulation model capable of reproducing the characteristics of the water surface oscillation revealed in this research. For the purposes of designing safer and more water friendly river structures.

ACKNOWLEDGMENTS

We would like to thank Dr. Jeremy D. Bricker of the Kobe University and Dr. George Lugomela of the Department of Water Resources, Tanzania for many fruitful suggestions and advice. The authors are pleased to acknowledge advice about POD analysis from Dr. H. Miyamoto of the Kobe University.

REFERENCES

1. Barron, J.L., D.J. Fleet and S.S Beauchemin : Performance of optical flow techniques, International Journal of Computer Vision, Vol.12, No.I, pp.43-77, 1994.

2. Berkooz, G., P. Golmes and J.L. Lumley : The proper orthogonal decomposition in the analysis of turbulent flows, Annual review of fluid mechanics, Vol.25, pp.539-575, 1993.

3. Chatterjee, A. : An introduction to the proper orthogonal decomposition, Current science, Vol.78, No.7, pp.808-817, 2000.

4. Cizmas, P.G., A. Palacios A, T. O'Brien and M. Syamlal : Proper-orthogonal decomposition of spatio-temporal patterns in fluidized beds, Chemical Engineering Science, Vol.58, pp.4417-4427, 2003.

5. Horn, B.K.P. and B.G. Schunck : Determining Optical Flow, MIT AI Memo, No.572, 1980.

6. Kimura, I. and T. Hosoda : Fundamental properties of flows in an open channel with a rectangular dead zone, Journal of Hydraulic Engineering, Vol.123, No.2, pp.98-107, 1997.

7. Raffel, M., C. Willert and J. Kompenhans : Particle Image Velocimetry, Springer-Verlag, Berlin, 1998.

8. Rockwell, D. and E. Naudascher : Review-Self-sustaining oscillations of flow past cavities, J. Fluids Eng., Vol.100, pp.152-165, 1978.

9. Rockwell, D. and E. Naudascher : Self-sustaining oscillations of impinging free shear layer, Annual Review of Fluid Mechanics, Vol.11, pp.67-94, 1979.

10. Rossiter, J.E. : Wind-tunnel experiments on the flow over rectangular cavities at subsonic and transonic speeds, Aeronautical Research Council Reports and Memoranda, No.3438, 1964.

11. Rowley, C.W., T. Colonius and R.M. Murray : POD based models of self-sustained oscillations in the flow past an open cavity, American Institute of Aeronautics and Astronautics, Paper 2000-1969, 2000.

12. Tsubaki, R. and I. Fujita : Measurements of water surface variations by using stereo video images, Annual journal of Hydraulic Engineering, Japanese society of civil engineers, Vol.48, pp.523-528, 2004(in Japanese).

13. Tsubaki, R. and I. Fujita : Stereoscopic measurement of afluctuating free surface with discontinuities, Meas. Sci. Technol., Vol.16, pp.1894-1902, 2005.

APPENDIX - NOTATION

The following symbols are used in this paper:

$a_k(x)$	=	temporal feature deomposed by POD;
Fr	=	froude number = $U/\sqrt{gH}$;
g	=	acceleration due to gravity (m^2/s);
$h(x,t)$	=	water depth distribution as function of space x and time t ;
H	=	mean depth of free surface flow (m);
$K(x,y)$	=	kernel ($E(h(x,y)h(y,t))$) used to calculate $\Phi_k(x)$;
L	=	wave length (m);
n	=	oscillation mode;
t	=	time coodinate;
T	=	period of oscillation (s);
U	=	mean velocity of main channel (m/s);
x	=	space coodinate;
λ	=	eigenvalue; and
$\Phi_k(x)$	=	spatial feature deomposed by POD.